Available online at www.sciencedirect.com
SCIENCE DIRECT®
Building and Environment 41 (2006) 1423–1434
BUILDING AND ENVIRONMENT
www.elsevier.com/locate/buildenv

Time-dependent analysis of RC frame structures considering construction sequences

Hyo-Gyoung Kwak*, Jin-Kook Kim

Department of Civil and Environmental Engineering, Korea Advanced Institute of Science and Technology, 373-1 Guseong-dong, Yuseong-gu, Daejeon 305-701, Korea

Received 3 December 2004; received in revised form 8 April 2005; accepted 11 May 2005

Abstract

This paper deals with a time-dependent analysis of reinforced concrete (RC) frame structures considering the construction sequences. Because of the non-mechanical deformations induced by the time-dependent deformations of concrete, concrete structures usually present different behaviors when the construction sequences are changed, despite having the same structural configurations. Therefore, the time-dependent effects of concrete such as creep and shrinkage must be taken into consideration to simulate the actual behavior of RC frame structures. The material nonlinearity including the cracking of concrete is taken into consideration, and geometric nonlinearity due to the P-Δ effect is also taken into account by using the initial stress matrix. In addition, the creep deformation of concrete is described in accordance with a first-order algorithm based on the expansion of a degenerated kernel of the compliance function. Finally, correlation studies with previous numerical results and experimental data are conducted to verify the validity of the proposed model. An analysis of a 10-story RC frame structure is carried out to assess the differences in structural responses according to the construction sequences.

Keywords: RC frame; Creep; Shrinkage; Construction sequence; P-Δ effect

1. Introduction

In the structural analysis of multistory buildings, there are two important factors that have very significant effects on the accuracy of the analysis but are usually ignored in practice [1]. They are: (1) the effect of sequential application of dead loads due to the sequential nature of construction; and (2) differential column shortening due to the different tributary areas that the exterior and interior columns support.

Structural members are added in stages as the construction of a building proceeds and hence their dead load is carried by the part of the structure completed at the stage of their installation. Therefore, it is clear that the distribution of displacements and stresses in the part of the structure completed at any stage due to the dead load of members installed by that stage does not depend on the sizes, properties, or the presence of members composing the remainder of the structure. The correct distribution of the displacements and stresses of any member can be obtained by accumulating the results of analysis of each stage. Ignoring this effect may lead to seriously incorrect analysis results, particularly at the upper floors of the building.

The exterior column in a building is loaded with roughly one-half of the gravity load to which the interior column is subjected. In many design practices, however, there is a tendency to design the exterior columns so as to have cross-sectional areas nearly equal to the interior ones, since additional cross-sections are required in the exterior columns to resist the forces induced by

*Corresponding author. Fax: +82 42 869 3610.
E-mail addresses: 1khg@kaist.ac.kr (H.-G. Kwak), glory95@kaist.ac.kr (J.-K. Kim).

0360-1323/$ - see front matter © 2005 Published by Elsevier Ltd.
doi:10.1016/j.buildenv.2005.05.013

overturning moments due to lateral loads such as winds and earthquakes. Therefore, there exists a substantial inequality between the ratio of the applied dead load to the cross-sectional area of an exterior column and that of an interior one. This inequality may cause a differential shortening between the exterior and interior columns in the frame. Moreover, this differential shortening is enlarged in RC frame structures since additional time-dependent deformations of concrete, which have a magnitude of more than two times the elastic deformation, are accompanied.

Because of the aforementioned two factors, considerable amounts of differential column shortening are accumulated in the members of the upper floors of a multistory building and cause larger bending moments and shear forces than when the dead load analysis for the frame is performed by a conventional method, such as a finite element analysis where the entire frame is assumed to resist all the applied loads instantaneously. In spite of the importance of considering the construction sequence and differential column shortening, and that the seriousness of this issue has long been recognized among many practicing engineers, only limited attention has been directed toward this problem in the current literature [2–4].

Accordingly, to simulate the structural behavior and to predict the exact structural responses, a rigorous numerical analysis considering the time-dependent deformations of concrete and construction sequence must be conducted. Upon these considerations, a numerical model that can consider all these influencing factors is introduced in this paper. The layer approach is adopted to simulate the different material properties across the sectional depth. Material nonlinearity due to the cracking of concrete and yielding of reinforcing bars, and geometric nonlinearity due to the P-Δ effect are taken into account. Concrete creep is evaluated by the first-order algorithm based on the expansion of the compliance function [5], and the aging effect of concrete properties is included in the evaluation. The validity of the numerical model introduced in this paper is established by comparing the analytical predictions with results from previous analytical and experimental studies [6–9], and numerical analyses for RC frame structures are conducted. On the basis of the obtained numerical results, the necessity of rigorous nonlinear analysis is emphasized for more accurate prediction of the structural response of RC frame structures.

2. Material properties

2.1. Concrete

Based on the principle of superposition, total uniaxial concrete strain $\varepsilon_c(t)$ at any time t is assumed to be composed of the mechanical strain $\varepsilon_c^{\mathrm{m}}(t)$ caused by short-term service loads, and the nonmechanical strain $\varepsilon_c^{\mathrm{nm}}(t)$ consists of creep strain $\varepsilon_c^{\mathrm{cr}}(t)$ and shrinkage strain $\varepsilon_c^{\mathrm{sh}}(t)$.

$$\varepsilon_c(t) = \varepsilon_c^{\mathrm{m}}(t) + \varepsilon_c^{\mathrm{nm}}(t) = \varepsilon_c^{\mathrm{m}}(t) + \varepsilon_c^{\mathrm{cr}}(t) + \varepsilon_c^{\mathrm{sh}}(t). \tag{1}$$

Shrinkage strain can be evaluated directly by utilizing the shrinkage model proposed in the ACI318 design code [10], since it is defined as the volume change that occurs independently of imposed stresses. On the other hand, creep is defined as an increase in strain under sustained stress. Introduction of an analytical model to calculate the creep strain is required, and many studies have been performed to this end [11,5]. In this paper, the first-order algorithm based on expansion of creep compliance, proposed by Kabir and Scordelis [5], has been adopted because this model can simulate the stress history effectively in spite of its simplicity in application.

The increment of creep strain from time t_{n-1} to time t_n for uniaxial stress state can be expressed as follows [11]:

$$\Delta\varepsilon_n^{\mathrm{c}} = \sum_{i=1}^{m} A_{i_{n-1}}(1 - \mathrm{e}^{-\lambda_i \Delta t_n}),$$
$$A_{i_n} = A_{i_{n-1}} \mathrm{e}^{-\lambda_i \Delta t_n} + a_i(\tau)\Delta\sigma_n, \tag{2}$$

where $\Delta\varepsilon_n^{\mathrm{c}}$ is the increment of creep strain, λ_i are inverse retardation times, $a_i(\tau)$ are constants depending on the age at loading τ, m is the number of time steps, and A_i with initial values $A_{i_1} = a_i(t_1) \cdot \Delta\sigma_1$ at $n = 1$ represent hidden state variables by which the effects of past time steps are considered.

Before starting the calculation of creep strain by Eq. (2), parameters such as m, $a_i(\tau)$, and λ_i must be determined. Since the use of the compliance function $(J(t,\tau) = 1/E(t) + C(t,\tau))$ in the form of a Dirichlet series induces some numerical difficulties caused by not considering a separate term to represent the instantaneous deformation, the creep compliance $(C(t,\tau))$ is used directly in this study, as shown in Eq. (3). Accordingly, $m = 4$ is taken, and the assumed corresponding retardation times are $8.0, 80.0, 800.0$, and 8000.0, respectively. In addition, the values of $a_i(\tau)$ are determined by the method of least squares using Kabir's Dirichlet series creep compliance [5]. After determination of nonmechanical strain increments, the concrete stress at each layer corresponding to the mechanical strain can be calculated by using the stress–strain relation of concrete.

$$C(t,\tau) = \sum_{i=1}^{m} a_i(\tau) \cdot [1 - \mathrm{e}^{-\lambda_i(t-\tau)}]. \tag{3}$$

The response of RC columns under loads depends to a large extent on the stress–strain relation of the constituent materials and the magnitude of stress. Since concrete is used mostly in compression, the stress–strain relation in compression is of primary interest. Among the many mathematical models currently used in the

analysis of RC structures, the monotonic envelope curve introduced by Kent and Park and later extended by Scott et al. [12] is adopted in this paper because of its simplicity and computational efficiency. In this model, as shown in Fig. 1(a), the monotonic concrete stress–strain relation in compression is described by three regions, where ε_{c0} is the concrete strain at maximum stress, K is a factor which accounts for the strength increase due to confinement, and Z is the strain softening slope.

On the other hand, it is assumed that concrete is linearly elastic in the tension region. Beyond the tensile strength, the tensile stress decreases linearly with increasing principal tensile strain (see Fig. 1(b)). Ultimate failure is assumed to take place due to cracking, when the principal tensile strain exceeds the value $\varepsilon_0 = 2G_f/f_t \ln(3/b)/(3-b)$ in Fig. 1(b), where b is the element length. G_f is the fracture energy that is dissipated in the formation of a crack of unit length per unit thickness and is considered to be a material property. The value of ε_0 is derived from the fracture mechanics concept of equating the crack energy release with the fracture toughness of concrete G_f [13]. The experimental study by Welch and Haismen [14] indicates

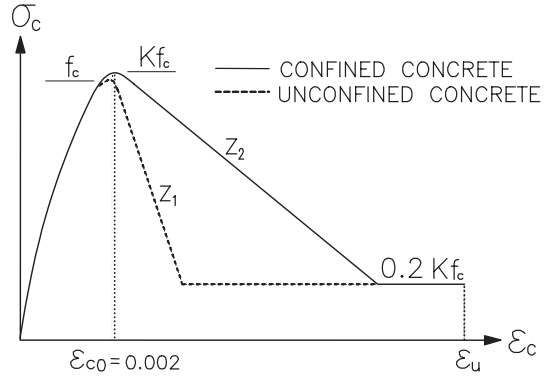

(a)

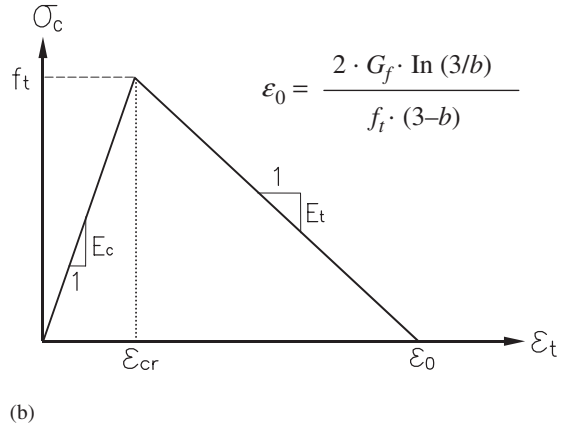

(b)

Fig. 1. Stress–strain relation of concrete. (a) Compressive region [12]; (b) Tensile region [13].

that for normal strength concrete, the value of G_f/f_t is in the range of 0.005–0.01 mm. If G_f and f_t are known from measurements, ε_0 can be directly determined from the equation in Fig. 1. More details for the concrete model can be found elsewhere [13,15].

2.2. Steel

Reinforcing steel is modeled as a linear elastic, linear strain hardening material with yield stress f_y. The reasons for this approximation are: (1) the computational convenience of the model; and (2) the behavior of RC members is greatly affected by the yielding of reinforcing steel when the structure is subjected to a monotonic bending moment [16,17]. Thermal strain is the only nonmechanical strain expected for steel. However, it is not considered in this study, and thus the mechanical strain can be directly calculated from the total strain of steel ($\varepsilon_s(t) = \varepsilon_s^{\mathrm{m}}(t)$).

3. Determination of neutral axis

In order to formulate the constitutive relationships in the section of an RC column, the following simplified assumptions have been made: (1) the section of an element is divided into imaginary layers to describe the different material properties; (2) plane sections remain plane to represent the linearity in the strain distribution on any section at any loading history; (3) a perfect bond between the concrete matrix and reinforcing bars is assumed; and (4) the constitutive materials are assumed to carry uniaxial stress only. In addition, shear deformation is not taken into account in the formulation because the shear effect is expected to be very small in slender RC columns.

Unlike a beam element subjected to a bending moment only, a column element is subjected to both axial force and bending moments and hence the neutral axis of a column section cannot be calculated directly by the equilibrium condition of normal force only. To determine the neutral axis while considering bending effects, the occurred mechanical strains of concrete ($\varepsilon_c^{\mathrm{m}}$) and steel ($\varepsilon_s^{\mathrm{m}} = \varepsilon_s^t$) need to be partitioned into an axial strain ($\varepsilon_{ca}^{\mathrm{m}}$, ε_{sa}^t) and a bending strain ($\varepsilon_{cb}^{\mathrm{m}}, \varepsilon_{sb}^t$), as represented in Fig. 2.

Since the axial strain is constant across the section and the bending strain vanishes at the neutral axis, the bending strains of concrete and steel at any layer can be calculated by $\varepsilon_{cb}^{\mathrm{m}} = \varepsilon_c^{\mathrm{m}} - \varepsilon_{ca}^{\mathrm{m}} = \varepsilon_c^t - \varepsilon_c^{\mathrm{nm}} - \varepsilon_{ca}^{\mathrm{m}}$, and $\varepsilon_{sb}^t = \varepsilon_s^t - \varepsilon_{sa}^t$, respectively. Based on the assumed neutral axis, the corresponding stress to the mechanical bending strain can be calculated from the stress–strain curves of the constitutive materials, and iterations using the bisection method are repeated until errors for the axial

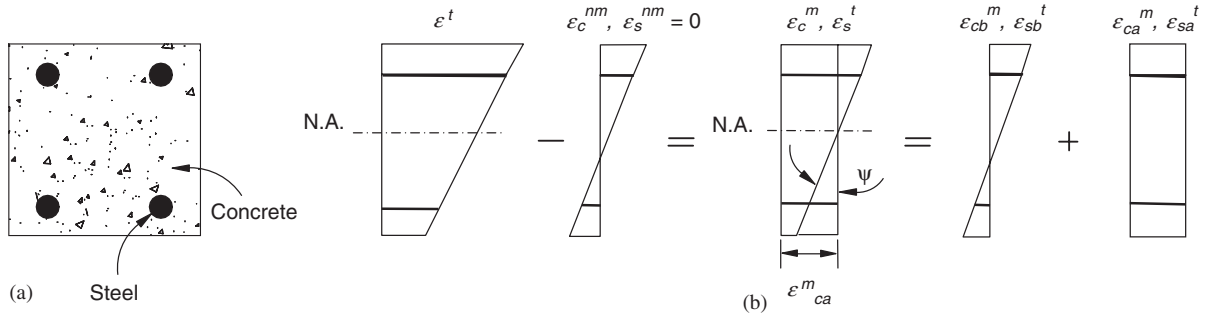

Fig. 2. Strain components at a section. (a) An RC column section, (b) Strain components.

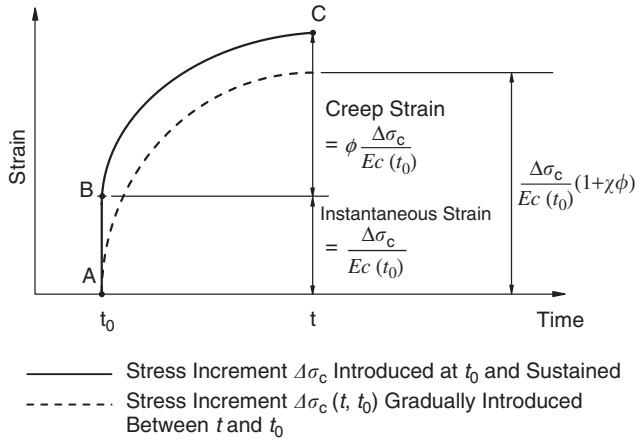

Fig. 3. Time variation of strain caused by a stress increment $\Delta\sigma_c$.

force and bending moment calculated by the axial strain and bending strain are within the given tolerances [18].

In addition, time rate in a stress increment has been considered. If a stress increment $\Delta\sigma_c(t_0)$ is introduced at time t_0 and sustained without a change in magnitude, the time variation of strain in concrete follows the continuous line ABC in Fig. 3, and the total strain at time t, instantaneous plus creep, can be represented by

$$\Delta\varepsilon_c^{\mathrm{cr}}(t) = \frac{\Delta\sigma_c(t_0)}{E_c(t_0)}(1+\phi), \tag{4}$$

where $\phi = \phi(t, t_0)$ is the creep coefficient.

On the other hand, when a stress increment $\Delta O_c(t, t_0)$ is gradually introduced between t_0 and t, the strain variation with time can be represented by the dashed line in Fig. 3. The total strain produced during the period $t_0 \sim t$ can be obtained by

$$\Delta\varepsilon_c^{\mathrm{cr}}(t, t_0) = \frac{\Delta\sigma_c(t_0, t_0)}{E_c(t_0)}(1+\chi\phi), \tag{5}$$

where χ is the concrete aging coefficient which accounts for the effect of aging on the ultimate value of creep for stress increments or decrements occurring gradually after the application of the original load. It is found that an average value of $\chi = 0.82$ can be used for most practical problems where the creep coefficient lies between 1.5 and 3.0 and t_0 is greater than 5 days. An approximate value of 0.8 has frequently been used for χ, and a value of $\chi = 0.82$ is adopted in this study [19].

4. Formulation of equilibrium equations

The equilibrium equations are derived on the basis of the assumed displacement field. As shown in Fig. 4, the nodal displacement vectors of a two-dimensional beam element in its local coordinate system can be expressed by $\boldsymbol{u} = \{u_1, u_2\}^{\mathrm{T}}$, $\boldsymbol{v} = \{v_1, v_2\}^{\mathrm{T}}$, and $\boldsymbol{\theta} = \{\theta_1, \theta_2\}^{\mathrm{T}}$ and the nodal displacements of an element may be expressed as the column vector $\boldsymbol{r} = \{\boldsymbol{u}, \boldsymbol{v}, \boldsymbol{\theta}\}^{\mathrm{T}}$.

Assuming that the independent axial displacement $U_0(x)$ varies linearly with x, and that the small rotation $\boldsymbol{\theta}_i$ at each node can be calculated by derivation of the vertical displacement v_i with respect to x, the displacements, $U_0(x)$ and $V(x)$ at any point within the element can be represented by

$$U_0(x) = \phi \cdot \boldsymbol{u}, \quad V(x) = \psi \cdot \begin{Bmatrix} \boldsymbol{v} \\ \boldsymbol{\theta} \end{Bmatrix}, \tag{6}$$

where $\phi = [(1-p), p]$ and $\psi = [(1-3p^2+2p^3), (3p^2-2p^3), L(p-2p^2+p^3), L(-p^2+p^3)]$ represent the displacement shape functions. The non-dimensional parameter p denotes x/L.

The displacements $U(x, y)$ and $V(x)$ can be expressed at any point as

$$\begin{aligned} U(x,y) &= U_0(x) - y\frac{\mathrm{d}V(x)}{\mathrm{d}x} = \phi \cdot u - y \cdot \psi_{,x} \begin{Bmatrix} v \\ \theta \end{Bmatrix} \\ &= [\phi, -y\psi_{,x}] \cdot \boldsymbol{r}, \\ V(x) &= [0, \psi] \cdot \boldsymbol{r}, \end{aligned} \tag{7}$$

where $\psi_{,x}$ is the first order derivative of ψ with respect to x.

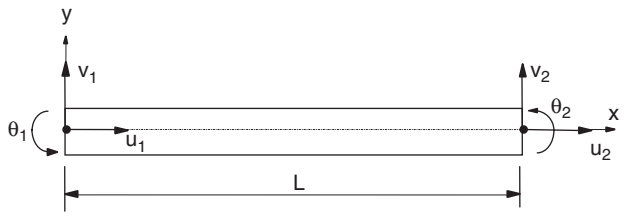

Fig. 4. Displacement components in a beam element.

In addition, the axial strain $\varepsilon(x, y)$ can be defined by

$$\varepsilon(x,y) = \frac{\mathrm{d}U(x,y)}{\mathrm{d}x} + \frac{1}{2}\left(\frac{\mathrm{d}V(x)}{\mathrm{d}x}\right)^2, \tag{8}$$

where the second term represents the nonlinear displacement effect.

A finite change in the joint displacement $\Delta \boldsymbol{r}$ induces the corresponding changes in the strain $\Delta\varepsilon$ such that

$$\begin{aligned}\Delta\varepsilon &= \frac{\mathrm{d}\Delta U}{\mathrm{d}x} \\ &= \left[\phi_{,x}, -y\psi_{,xx}\right]\cdot\Delta\boldsymbol{r} + \frac{1}{2}\Delta\boldsymbol{r}^{\mathrm{T}}\cdot[0,\psi_{,x}]^{\mathrm{T}}\cdot[0,\psi_{,x}]\cdot\Delta\boldsymbol{r} \\ &= \boldsymbol{B}\cdot\Delta\boldsymbol{r} + \frac{1}{2}\Delta\boldsymbol{r}^{\mathrm{T}}\cdot\boldsymbol{c}^{\mathrm{T}}\cdot\boldsymbol{c}\cdot\Delta r,\end{aligned} \tag{9}$$

where

$$\begin{aligned}\boldsymbol{B} &= [\phi_{,x}, -y\psi_{,xx}] \\ &= \left[-\frac{1}{L}, \frac{1}{L}, y(1-2p)\frac{6}{L^2}, y(-1+2p)\frac{6}{L^2},\right. \\ &\quad \left. y(2-3p)\frac{2}{L}, y(1-3p)\frac{2}{L}\right].\end{aligned}$$

Moreover, the incremental strain–displacement relationship of $\mathrm{d}\boldsymbol{\varepsilon} = \boldsymbol{B}\cdot\mathrm{d}\boldsymbol{r} + \mathrm{d}\boldsymbol{r}^{\mathrm{T}}\cdot\boldsymbol{c}^{\mathrm{T}}\cdot\boldsymbol{c}\cdot\Delta\boldsymbol{r} = \mathrm{d}\boldsymbol{r}^{\mathrm{T}}\cdot(\boldsymbol{B} + \boldsymbol{c}^{\mathrm{T}}\cdot\boldsymbol{c}\cdot\Delta\boldsymbol{r})$ can be developed by taking the differential from Eq. (9).

Applying the virtual work principle of $\mathrm{d}\boldsymbol{r}^{\mathrm{T}}\cdot(\boldsymbol{R}^j + \Delta\boldsymbol{R}^j) = \int_V \mathrm{d}\varepsilon\cdot(\sigma+\Delta\sigma)\,\mathrm{d}V$ to a finite element on the basis of the virtual displacement $\mathrm{d}\boldsymbol{r}$ and neglecting a higher order incremental term, the incremental of nodal force vector $\Delta\boldsymbol{R}^j$ applied at node j can be written from Eq. (9) as

$$\begin{aligned}\Delta\boldsymbol{R}^j &= \int_V \boldsymbol{B}^{\mathrm{T}}\Delta\sigma\,\mathrm{d}V + \int_V \boldsymbol{c}^{\mathrm{T}}\sigma\boldsymbol{c}\,\mathrm{d}V\cdot\Delta\boldsymbol{r} \\ &= \int_V \boldsymbol{B}^{\mathrm{T}}E(\mathrm{d}\varepsilon^t - \mathrm{d}\varepsilon^{\mathrm{nm}})\,\mathrm{d}V + \int_V \boldsymbol{c}^{\mathrm{T}}\sigma\boldsymbol{c}\,\mathrm{d}V\cdot\Delta\boldsymbol{r} \\ &= \left[\int_V \boldsymbol{B}^{\mathrm{T}}E\boldsymbol{B}\,\mathrm{d}V + \int_V \boldsymbol{c}^{\mathrm{T}}\sigma\boldsymbol{c}\,\mathrm{d}V\right]\cdot\Delta\boldsymbol{r} \\ &\quad - \int_V \boldsymbol{B}^{\mathrm{T}}E\,\mathrm{d}\varepsilon^{\mathrm{nm}}\,\mathrm{d}V,\end{aligned} \tag{10}$$

where E is the tangent modulus of the constitutive material.

Finally, the equilibrium equations can be rewritten in differential form as

$$\mathrm{d}\boldsymbol{R} = \mathrm{d}\boldsymbol{R}^j + \mathrm{d}\boldsymbol{R}^{\mathrm{nm}} = [\boldsymbol{K}]\cdot\mathrm{d}\boldsymbol{r}, \tag{11}$$

where $[\boldsymbol{K}] = [\boldsymbol{K}_{\mathrm{e}}] + [\boldsymbol{K}_{\mathrm{g}}] = \int_V \boldsymbol{B}^{\mathrm{T}}E\boldsymbol{B}\,\mathrm{d}V + \int_V \boldsymbol{c}^{\mathrm{T}}\sigma\boldsymbol{c}\,\mathrm{d}V$, $[\boldsymbol{K}_{\mathrm{e}}] = \int_V \boldsymbol{B}^{\mathrm{T}}E\boldsymbol{B}\,\mathrm{d}V$, $[\boldsymbol{K}_{\mathrm{g}}] = \int_V \boldsymbol{c}^{\mathrm{T}}\sigma\boldsymbol{c}\,\mathrm{d}V$, $\mathrm{d}\boldsymbol{R}^{\mathrm{nm}} = \int_V \boldsymbol{B}^{\mathrm{T}}E\,\mathrm{d}\varepsilon^{\mathrm{nm}}\,\mathrm{d}r$,

$$[\boldsymbol{K}_{\mathrm{g}}] = \begin{bmatrix} EA/L & -EA/L & 0 & 0 & 0 & 0 \\ & EA/L & 0 & 0 & 0 & 0 \\ & & 12EI/L^3 & -12EI/L^3 & 6EI/L^2 & 6EI/L^2 \\ & & & 12EI/L^3 & -6EI/L^2 & -6EI/L^2 \\ & sym. & & & 4EI/L & 2EI/L \\ & & & & & 4EI/L \end{bmatrix}, \tag{12}$$

$$[\boldsymbol{K}_{\mathrm{g}}] = \begin{bmatrix} 0 & 0 & 0 & 0 & 0 & 0 \\ & 0 & 0 & 0 & 0 & 0 \\ & & 6P/5L & -6P/5L & P/10 & -P/10 \\ & & & 6P/5L & -P/10 & -P/10 \\ & sym. & & & 2PL/15 & -PL/30 \\ & & & & & 2PL/15 \end{bmatrix}. \tag{13}$$

while calculating the elastic stiffness $[K_{\mathrm{e}}]$ and the geometric stiffness $[K_{\mathrm{g}}]$, the value of E at each layer is assumed to be held constant along the element length, and thus the volume integration in Eq. (10) can be represented by the inner product of the line integration along the element length and the area integration across the sectional depth. Moreover, since the layer approach is employed, wherein a typical section is divided into imaginary layers, the sectional stiffness terms of EA and EI in Eq. (12) can be evaluated by summation over all layers. $EA = \int_A E\,\mathrm{d}A = \sum_{i=1}^{n_c} E_{c_i}A_{c_i} + \sum_{i=1}^{n_s} E_{s_i}A_{s_i}$ and $EI = \int_A Ey^2\,\mathrm{d}A = \sum_{i=1}^{n_c} E_{c_i}y_{c_i}^2A_{c_i} + \sum_{i=1}^{n_s} E_{s_i}y_{s_i}^2A_{s_i}$, where n_c and n_s denote the number of concrete and steel layers respectively, A_i and E_i are the sectional area and elastic modulus of the ith layer, y_i is the distance from the centroid, and P refers to the applied force.

5. Solution algorithm

Every nonlinear analysis algorithm consists of four basic steps: the formation of the current stiffness matrix, the solution of the equilibrium equations for the displacement increments, the state determination of all elements in the model, and a convergence check. These steps are presented in some detail in the flow diagram of Fig. 5. Since the global stiffness matrix of the structure depends on the displacement increments, the solution of the equilibrium equations is typically accompanied by an iterative method through the convergence check. The nonlinear solution scheme selected in this paper uses the tangent stiffness matrix at the beginning of each load

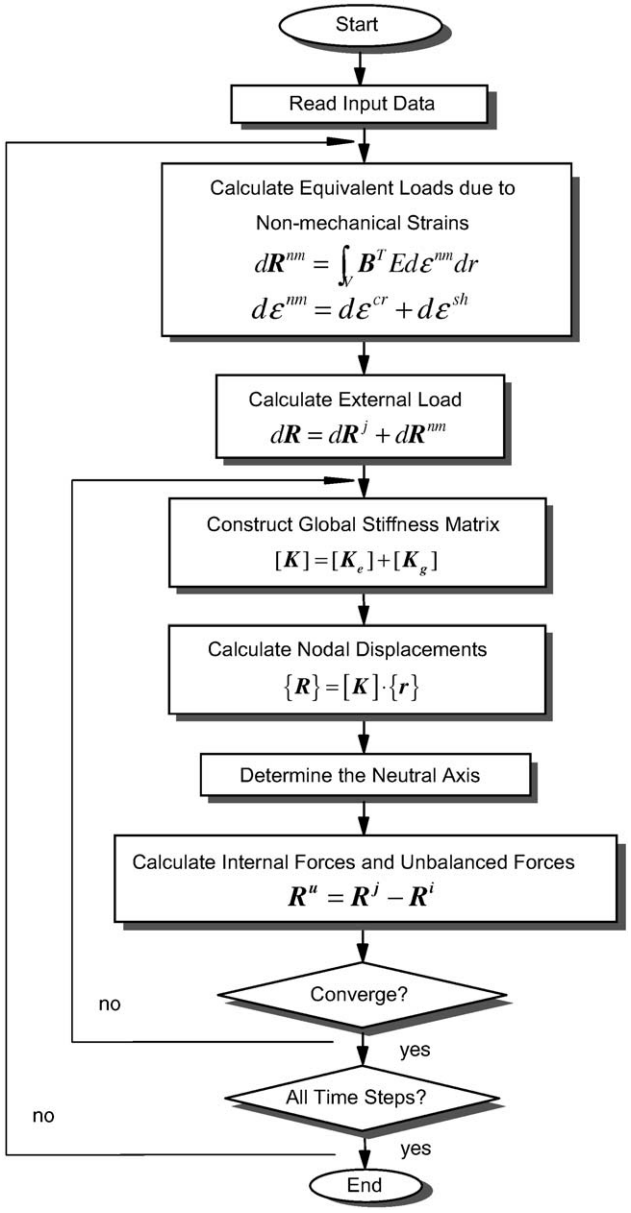

Fig. 5. Solution procedure.

step and each time step in combination with a constant stiffness matrix during the subsequent correction phase; that is, an incremental-iterative method.

The criteria for measuring the convergence of the iterative solution are generally based on the accuracy of satisfying the global equilibrium equations or on the accuracy of determining the total displacements. The accuracy of satisfying the global equilibrium is controlled by the magnitude of the unbalanced nodal forces. Hence the convergence criteria for the unbalanced nodal forces are used in this paper, and these can be expressed as

$$|F^{\max}_{\text{unbal.}}| \leqslant Tol._F, \quad |M^{\max}_{\text{unbal.}}| \leqslant Tol._M, \tag{14}$$

where $|F^{\max}_{\text{unbal.}}|$ and $|M^{\max}_{\text{unbal.}}|$, are the absolute values for the ratios of the maximum unbalanced axial force and bending moment to the internal axial force and bending moment, respectively, and $Tol._F$ and $Tol._M$ are the specified tolerances corresponding to the axial force and bending moment. $Tol._F = Tol._M = 0.02$ is adopted in this study, and more details for the solution procedures can be found elsewhere [18].

6. Analytical and experimental verification

6.1. Short-term loading

The experimental results from several hinged RC columns tested by Kim et al. [9] are adopted to investigate the validity of the analytical model introduced in this paper. More details of the material properties used and the experimental procedure for each specimen can be found elsewhere [9].

The ultimate loads of columns measured experimentally are compared with those obtained by the analytical model in Table 1. Good agreement is obtained for the individual columns, regardless of the compressive strength of concrete and the slenderness ratio, and thus it is concluded that the introduced numerical model can accurately predict the ultimate loads of hinged RC columns. In addition, Fig. 6, representing a typical relation between the axial force and lateral deflection at the mid-span, shows that the introduced numerical model not only gives accurate predictions for the ultimate load but also effectively simulates the nonlinear behavior of slender RC columns as the axial force increases.

An additional comparison with numerical calculations introduced by Bazant et al. [6,20] is conducted to

Table 1
Comparison of ultimate load of RC columns with test results by Kim et al. [9]

f'_c(kgf/cm^2)	L/r	Test results $P_{u,t}$ (Ton) (Kim et al.)	Analysis results $P_{u,a}$ (Ton) (This study)	$P_{u,a}/P_{u,t}$
259.9	60	6493	6600	1.02
		6697		0.99
	100	3894	3780	0.97
		3568		1.06
647.3	60	10,479	10,400	0.99
		11,570		0.90
	100	4608	4840	1.05
		4852		1.00
878.7	60	12,446	11,840	0.95
		12,610		0.94
	100	5535	5520	1.00
		5596		0.99

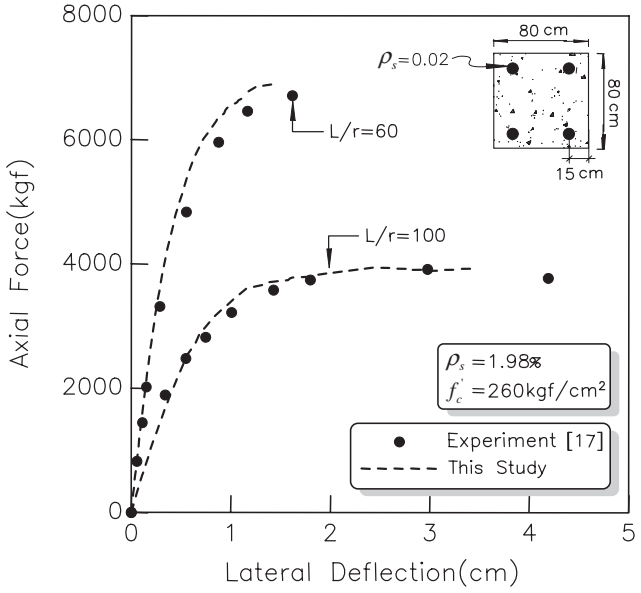

Fig. 6. Comparison with test results.

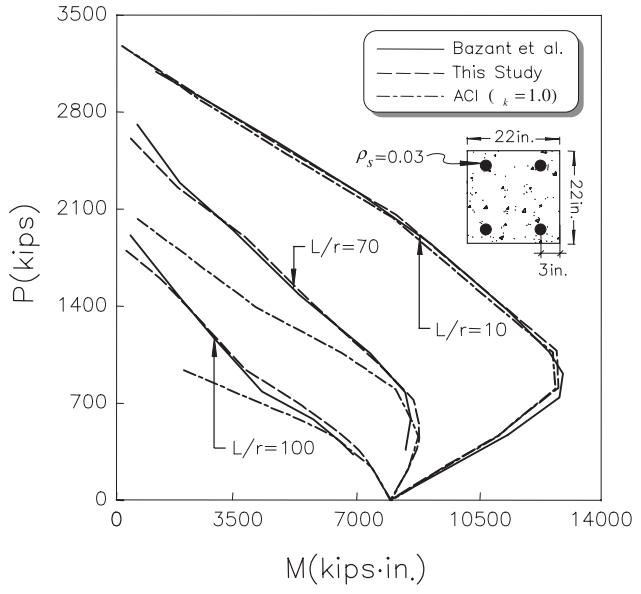

Fig. 7. Failure envelopes for pin-ended RC columns

verify the proposed numerical model. The steel ratio and cross-section dimensions of the adopted columns with slenderness ratios of $L/r = 10, 70$, and 100 are represented in Fig. 7. The same material properties of concrete and steel with those used in the previous analytical study [6] are used and have the following values: $f'_c = 5000$ psi (352 kg/cm^2), $E_s = 29 \times 10^6$ psi (2.04×10^6 kg/cm^2) and $f_y = 60\,000$ psi (4220 kg/cm^2).

For the design of slender RC columns, ACI-318 [10] recommends a simple approximate formula based on the moment magnification factor. When a column is subjected to ultimate loads of P_u and $M_u = P_u.e$, the load and moment used in the design of the column section are assumed to be P_u and $\delta \cdot M_u$, where δ is the moment magnification factor and is represented by $\delta = C_m/(1 - P_u/\phi_k \cdot P_{cr}) \geqslant 1$; P_{cr} is the elastic buckling load; and C_m is an equivalent moment correction factor ($C_m = 1$ in this example) [10].

Moreover, as noted in a previous study [21], the stiffness reduction factor ϕ_k, designed to consider the inevitable random variability of the materials, has not been incorporated for the purpose of comparison with the numerical results ($\phi_k = 1.0$ is assumed).

As shown in Fig. 7, the numerical results obtained represent good agreement with those obtained by Bazant et al. [6], leading to the conclusion that the proposed numerical model can accurately predict the ultimate loads of slender RC columns. From the numerical results for this example structure, the following can be inferred: (1) as the slenderness ratio increases, the difference between the ACI envelopes and the numerical results gradually increases; (2) the ACI method may underestimate the resisting capacity of slender RC columns; and (3) the ACI method does not achieve the objective of a uniform safety margin, that is, the uniform difference between the results predicted by the ACI method and the results calculated by a rigorous analysis over an entire eccentricity [6].

6.2. Long-term loading

To verify the efficiency of the introduced numerical model for long-term behavior, correlation studies between analytical and experimental results by Drysdale et al. [8] are conducted. The geometry and cross-section

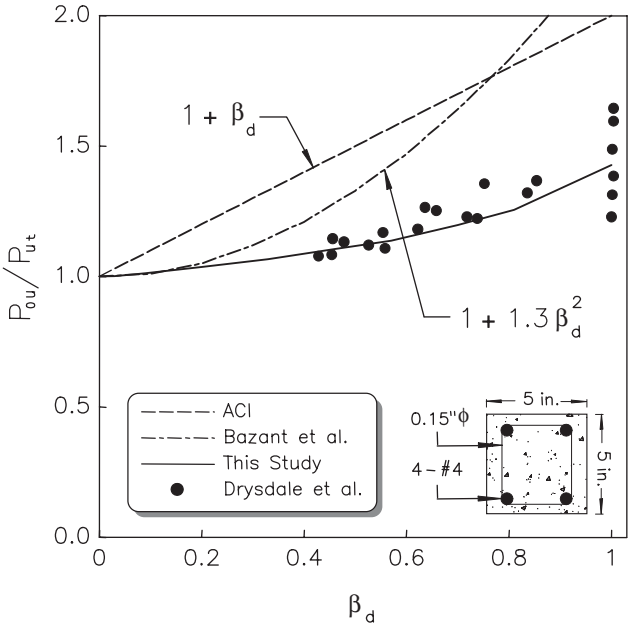

Fig. 8. Long-term resistance of RC columns.

dimensions of the tested columns are represented in Fig. 8, and the columns have a slenderness ratio of $L/r = 107$. Moreover, the following material properties, which have the same values with those used in the experiments, are adopted: $f'_c = 4000$ psi (282 kg/cm^2), $E_s = 29 \times 10^6$ psi (2.04×10^6 kg/cm^2), and $f_y = 56\,000$ psi (3940 kg/cm^2). To trace the time-dependent behavior of RC columns, creep and shrinkage of concrete are considered with the aging effect of concrete, and an ultimate creep coefficient of $c_u = 3.0$ and an ultimate shrinkage strain of $\varepsilon_{sh}^{\infty} = 600 \times 10^{-6}$ are assumed on the basis of the ACI model.

Fig. 8 shows a plot of P_{ou}/P_{ut} versus β_d where $\beta_d = P_D/(P_D + P_L)$ = the ratio of dead load to total load, P_{ou} = short-term failure load, and P_{ut} = long-term failure load. When an RC column is subjected to a small, sustained load, which means that β_d has a relatively small value, the points of failure caused by the subsequent sudden overload generally indicate a substantial increase in strength. This phenomenon, however, is almost nonexistent in the tests of Drysdale et al. because drying prevents the increase of concrete strength due to hydration. This means that the analytical results may represent lower values of P_{ou}/P_{ut} than those from the experimental data along the whole range of β_d, because the increase in concrete strength can effectively be considered in the numerical analyses by implementing the age effect. In this aspect, the two models proposed by the ACI and Bazant et al. give slightly conservative results and underestimate the resisting capacity of slender RC columns as β_d increases. Moreover, since the dead load takes possession of 50% of the total design load in most RC columns ($\beta_d \geqslant 0.5$), direct application of the ACI model or the Bazant model may result in a conservative design.

On the other hand, the numerical results from the introduced analytical model agree well with the experimental results. Particularly at $\beta_d = 1$, the numerical result shows a 30% reduction in the ultimate resisting capacity for the axial load. This coincides well with the experimental results, which represent reductions ranging from 20% to 40%.

More correlation studies between analytical results and experimental values from simply supported RC beam tests are conducted. These beams are specimens A1, A2, B1, and B2 tested by Clarke et al. [7] and are subjected to concentrated loads and bending moments at the one-third points of the structure. The geometry and configuration of the adopted beams are presented in Fig. 9, and the material properties and cross-section dimensions are summarized in Table 2. The loads act at age $t = 28$ days, and the long-term deflection at mid-span are investigated at age $t = 180$ days after application of the loads. Table 3 compares the analytical results with the measured mid-span deflections and with those of earlier analytical studies.

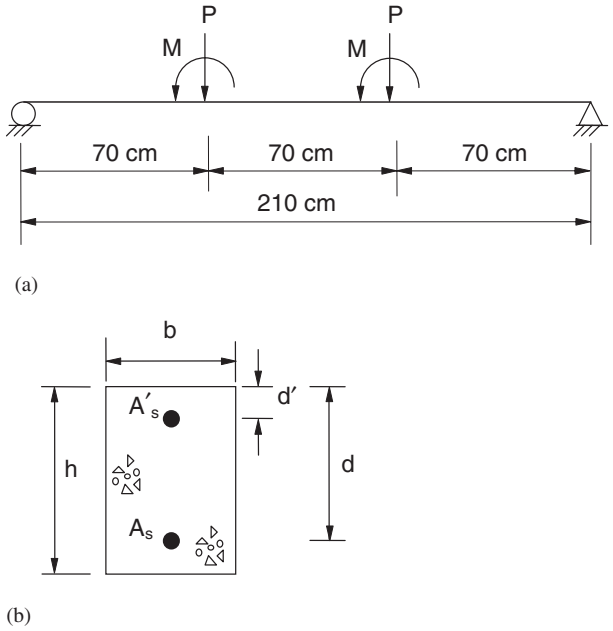

Fig. 9. A simply supported RC beam. (a) Elevation and (b) cross section.

Table 2
Material properties and cross-section dimensions in RC beams

Beam	*A*1	*A*2	*B*1	*B*2
b(cm)	10.0	10.0	10.0	10.0
d'(cm)	2.0	2.0	2.0	2.0
d(cm)	13.2	13.0	13.0	13.2
h(cm)	15.4	15.2	15.2	15.4
A_s(cm^2)	1.6	1.6	1.6	1.6
A'_s(cm^2)	—	—	1.6	1.6
P(kg)	510.2	510.2	510.2	510.2
M(kg-cm)	35,714.3	35,714.3	35,714.3	35,714.3
f'_c(kg/cm^2)	213.9	213.9	213.9	213.9
E_c(kg/cm^2)	2.2×10^5	2.2×10^5	2.2×10^5	2.2×10^5
E_s(kg/cm^2)	2.1×10^6	2.1×10^6	2.1×10^6	2.1×10^6
ϕ_∞	2.26	2.26	2.26	2.26

Table 3
Comparison of the analytical results

Beam		*A*1	*A*2	*B*1	*B*2
Short-term deflection (mm)	This Study	4.77	4.96	4.41	4.20
	Test [23]	4.89	5.09	4.78	4.30
Long-term deflection (mm)	Branson [24]	13.96	14.58	9.87	9.45
	Mayer [25]	7.85	8.22	5.94	5.69
	BS 8110 [26]	7.80	8.11	5.89	5.67
	Clarke et al. [7]	8.75	9.08	7.07	6.82
	This Study	9.30	9.74	7.01	6.73
	Test [23]	9.28	9.37	8.15	7.93

The long-term deflections obtained in the previous studies show significant differences from the experimental results, while very satisfactory agreements between analyses using the proposed numerical approach and experiments are obtained. Nevertheless, there is still some discrepancy between the experimental and analytical results for the long-term deformations. These differences seem to be caused by not considering the shrinkage effect in the analysis. Since material properties related to the shrinkage of concrete were not tested in the experiments, it may be almost impossible to exactly consider the shrinkage of concrete in the analysis. Through these correlation studies between analytical and experimental results, we found that the proposed numerical approach can be used effectively to trace the long-term behavior of RC frame structures.

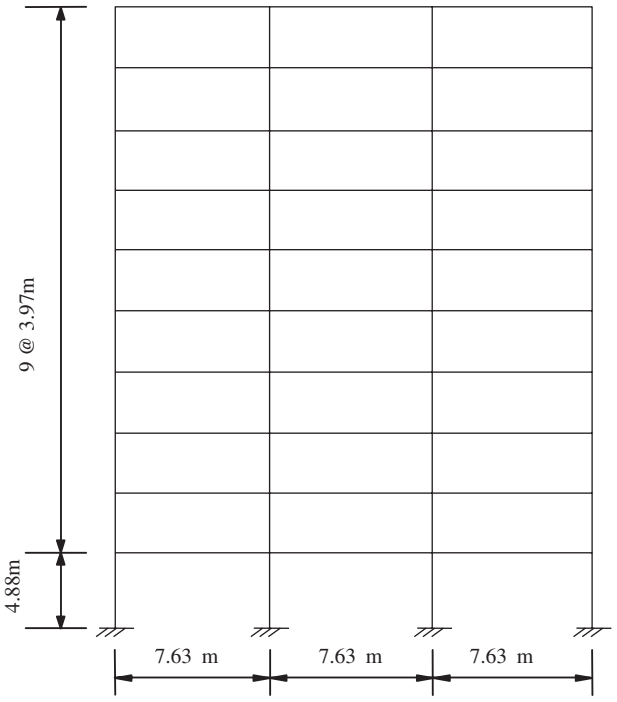

Fig. 10. Configuration of a 10-story RC frame.

7. 10-Story RC building frame

Unlike a conventional analysis on the basis of a completed frame structure, a real structure is sequentially constructed while accompanying continuous changes in the structural system with an increase in the number of degrees of freedom as a floor is constructed. Assuming that the building is constructed one floor at a time, a floor is constructed on the top of the frame that was completed at that particular stage of construction and in which the column shortening due to the dead weight already took place before construction of the floor commenced. Moreover, since each floor is leveled at the time of its construction, the deformations that occurred in the frame below are of no consequence.

In order to explain the structural behavior caused by the differences in the frame analysis procedures, a 10-story RC frame subjected only to gravity loads is analyzed. The same structure was also analyzed by Choi et al. [22]. The configuration for the frame is shown in Fig. 10, and the member dimensions for beams and columns are given in Table 4. The thickness of slabs is assumed to be 120 mm. Unlike the previous study [22], however, the long-term deformations of concrete are also taken into account in this paper. The compressive strength of concrete $f_c = 400\,\mathrm{kg/cm^2}$, the yielding strength of steel $f_y = 4000\,\mathrm{cm^2}$, and the steel ratios for columns $\rho_{sc} = 4\%$ and for beams $\rho_{sb} = 2.3\%$ are assumed. The ultimate creep coefficient ϕ_{cr}^{∞} and the ultimate shrinkage strain $\varepsilon_{sh}^{\infty}$ of concrete are assumed to be 3 and 300×10^{-6} for the interior members and 2 and 200×10^{-6} for the exterior members, respectively. Construction of each floor is sequentially constructed with a five-day interval and the self-weight of slabs acts on the frame structure after 20 days when the slab concrete is pored.

The curves in Fig. 11 show that there is virtually no difference between the results from the gravity analysis of the complete frame and the method of this study considering the construction sequence at the floors near the ground level and the discrepancy increases gradually

Table 4
Dimensions of RC members

Floor	Member	Width × Depth ($B \times H$) (cm)	Gross area of concrete (A_c) (cm^2)	Steel area (cm^2)
10	Beam	22.5 × 57.5	1293.8	$A_{st} = A_{sc} = 29.8$
7–9		22.5 × 60.0	1350.0	$A_{st} = A_{sc} = 31.1$
4–6		25.0 × 62.5	1562.5	$A_{st} = A_{sc} = 35.9$
1–3		25.0 × 65.0	1625.0	$A_{st} = A_{sc} = 37.4$
7–10	Column	25.0 × 40.0	1000.0	$A_s = 40.0$
6		25.0 × 42.5	1062.5	$A_s = 42.5$
5		25.0 × 47.5	1187.5	$A_s = 47.5$
3–4		27.5 × 50.0	1375.0	$A_s = 55.0$
2		27.5 × 52.5	1443.8	$A_s = 57.8$
1		32.5 × 60.0	1950.0	$A_s = 78.0$

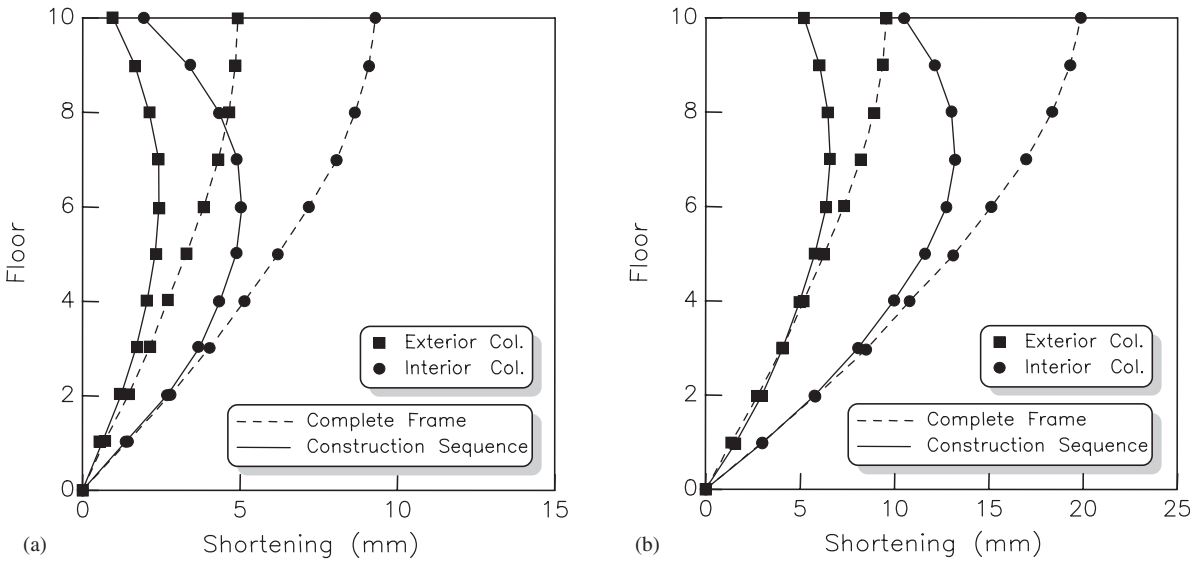

Fig. 11. Column shortening at a 10-story RC frame. (a) Without time-dependent deformations of concrete. (b) With time-dependent deformations of concrete.

to reach a maximum value at the top floors. More differences occurred in the interior columns where more gravity loads act, but the difference is not exactly proportional to the magnitude of the applied loads. In particular, the column shortenings at the top floor obtained by the method proposed in this study at $t = 65$ days are only fractions of those obtained by the gravity analysis of the complete frame. The column shortening in the interior columns is divided into each deformation component, and the result is shown in Fig. 12. Since the column is subjected to sequentially increased gravity loads, creep deformation of concrete is accompanied, and many design codes [2,3] require consideration of the creep deformation of concrete.

However, consideration of the shrinkage deformation of concrete is still not clearly mentioned in all design codes [2,3]. Fig. 12 shows that the shrinkage deformation increases the column shortening along the floor and may cause an increase of the bending moments in beams produced by the different column shortening. Accordingly, exact calculation of structural behavior must be based on a rigorous time-dependent analysis considering the long-term deformations of concrete.

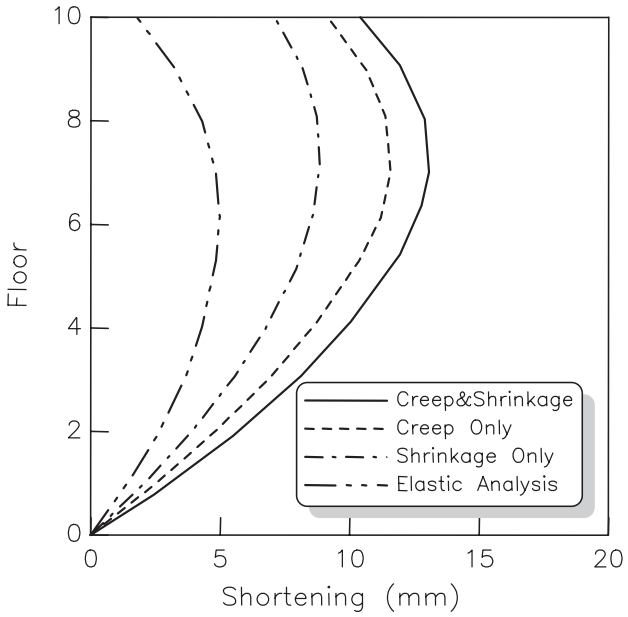

Fig. 12. Relative contribution of each deformation to column shortening at $t = 65$ days.

The differential vertical column shortenings between interior and exterior columns and the bending moments induced in the beams of the frame are shown in Fig. 13. The analytical results from the gravity analysis of the complete frame are represented with those obtained by considering the construction sequence only without additional consideration for the time-dependent deformations of concrete and those obtained using the method proposed in this paper for ease of comparison. From Fig. 13, the following can be inferred: (1) as shown in Fig. 11, the frame analysis considering the construction sequences represents remarkable differences in the column shortenings. In spite of such large differences in column shortenings, the differential column shortenings between the interior and exterior columns show relatively small differences between the two analysis methods; (2) greater differential column shortenings and bending moments are developed when the construction sequence and the time-dependent deformations of concrete are considered; (3) the time-dependent deformations of concrete increase the

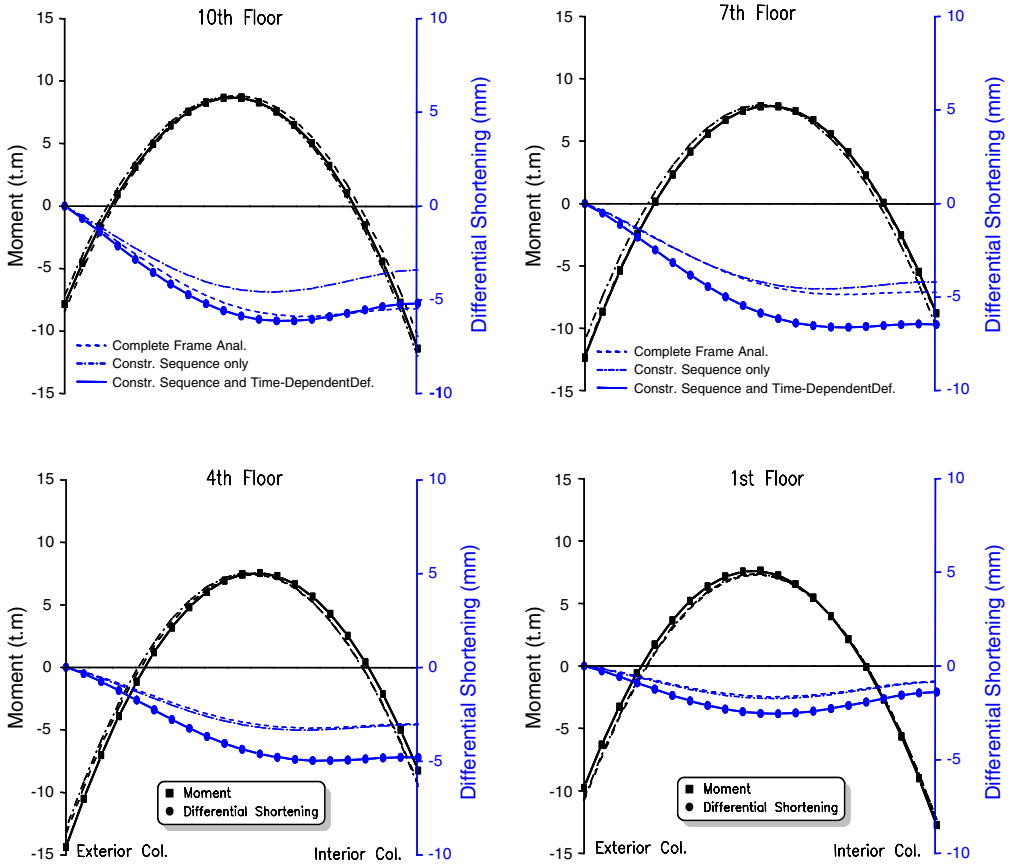

Fig. 13. Differential column shortenings and bending moments.

structural responses, but the magnitudes of the bending moments are not greatly varied. This means that the bending moments are still governed by the gravity loads; (4) in contrast to the bending moment distributions in the beams, the differential vertical column shortenings are increased even in this low-rise building structure due to the time-dependent deformations of concrete. This implies that more differential column shortenings will occur in the high-rise building structures, and there will be greater serviceability problems in the non-structural members located between interior and exterior columns, such as cracking in the masonry walls and windows. The results obtained in this paper have shown that differential column shortening should not be neglected in the analysis of frame structures, even in low-rise buildings. Some additional computational efforts in conducting a rigorous nonlinear analysis for more exact prediction of the structural responses can be justified.

8. Conclusions

A numerical model to simulate the time-dependent behavior of a RC frame structure considering the construction sequence is proposed in this paper, and the efficiency of the introduced model is verified by comparison with results from previous analytical and experimental studies. Moreover, on the basis of the numerical results in this limited investigation, the following conclusions are obtained: (1) greater differential column shortenings and bending moments are developed when the construction sequence and the time-dependent deformations of concrete are considered; and (2) greater serviceability problems in the nonstructural members located between interior and exterior columns are induced by the differential column shortenings while the bending moments in beam members due to the column shortenings are not significant.

A complete frame analysis without consideration of the construction sequence and time-dependent deformations of concrete usually underestimates the structural responses. Therefore, to cope with the serviceability problems in nonstructural members, a rigorous time-dependent nonlinear analysis considering the construction sequence must be performed at the final design stage of a building structure. As such, sophisticated numerical methods considering all the nonlinearities will play an increasingly important role and will become the standard for final design checks in a high-rise building structure.

Acknowledgements

The authors would like to thank the Infra-Structures Assessment Research Center (ISARC) funded by Korea Ministry of Construction and Transportation (MOCT) for financial support.

References

[1] Choi CK, Chung HK, Kim ED. Integrated building design system (part 1)—linear three dimensional analysis. In: SEMR 89-01. Seoul: Dept. of Civil Eng., KAIST, 1989. p. 52–68.
[2] ACI committee 347 Guide to Formwork for Concrete. (ACI 347-02). Detroit: American Concrete Institute; 2002.
[3] Australian Standard (AS) Formwork for concrete AS3610-95. Sydney: Australian Standard; 1995.
[4] El-shahhat AM, Chen WF. Improved analysis of shore-slab interaction. ACI Structural Journal 1992;89(5):528–37.
[5] Kabir AF. Nonlinear analysis of reinforced concrete panels. In: Slabs and shells for time dependent effects Report No. UC-SEEM 76-6. Berkeley: University of California; 1976.
[6] Bazant ZP, Xiang Y. Inelastic buckling of concrete column in braced frame. Journal of Structural Engineering 1997;123(5): 634–42.
[7] Clarke GS, Scholz H, Alexander M. New method to predict the creep deflection of cracked reinforced concrete flexural members. ACI Material Journal 1988;85(2):95–101.
[8] Drysdale RG, Huggins MW. Sustained biaxial load on slender concrete columns. Journal of Structural Division ASCE 1971;97(ST5):1423–43.
[9] Kim JK, Yang JK. Buckling behaviour of slender high-strength concrete columns. Engineering Structures 1995;17(1):39–51.
[10] ACI Committee 318 Building Code Requirements for Reinforced Concrete (ACI 318-99). Detroit: American Concrete Institute; 1999.
[11] Bazant ZP, Wu ST. Dirichlet series creep function for aging concrete. Journal of Engineering. Mechanics ASCE 1973; 99(EM2):367–87.
[12] Scott BD, Park R, Priestley MJN. Stress–strain behavior of concrete confined by overlapping hoops at low and high strain rates. ACI 1982;79(1):13–27.
[13] Kwak HG, Filippou FC. Finite element analysis of reinforced concrete structures under monotonic loads Report No. UCB/SEMM-90/14. Berkeley: University of California; 1990.
[14] Welch GB, Haisman B. Fracture toughness measurements of concrete. In: Report No. R42. Sydney: University of New South Wales; 1969.
[15] Kwak HG, Kim SP. Bond-slip behavior under monotonic uniaxial loads. Engineering Structures 2001;23(3):298–309.
[16] Ngo D, Scordelis AC. Finite element analysis of reinforced concrete beams. ACI 1967;64(3):152–63.
[17] Vedo A, Ghali A. Moment-curvature relation of reinforced concrete slabs. Journal of Structural Division ASCE 1977;103(3): 515–31.
[18] Kwak HG, Seo YJ. Long-term behavior of composite girder bridges. Computers and Structures 2000;74(5):583–99.
[19] Neville AM, Dilger WH, Brooks JJ. Creep of plain and structural concrete. London and New York: Construction Press; 1982.
[20] Bazant ZP, Cedolin L, Tabbara MR. New method of analysis for slender columns. ACI Structural Journal 1991;88(4):391–401.
[21] Mirza SA, Lee PM, Morgan DL. ACI stability resistance factor for RC columns. Journal of Structural Engineering ASCE 1987;113(9):1963–76.
[22] Choi CK, Kim ED. Multistory frames under sequential gravity loads. Journal of Structural Engineering ASCE 1985;111(11): 2373–84.
[23] Clarke GS. Long-term deflection of reinforced concrete flexural elements. MSc thesis. Johannesburg: University of the Witwatersrand; 1987.
[24] Branson DE. Deformation of concrete structures. New York: McGraw-Hill Book Co.; 1977.
[25] Mayer H. Die berechnung der durchbiegung von Stahlbeton-Bauteilen. In: Bulletin No. 194. Berlin: Duetscher Ausschuss für Stahlbeton, 1967. p. 73.
[26] BS8110 Structural Use of Concrete. Part 1. Code of Practice for Design and Construction. London: British Standards Institution; 1985.